

A deep convolutional neural network for burn progression mapping using Sentinel-1 SAR time-series

Ali Radman, Reza Shah-Hosseini & Saeid Homayouni

To cite this article: Ali Radman, Reza Shah-Hosseini & Saeid Homayouni (2023) A deep convolutional neural network for burn progression mapping using Sentinel-1 SAR time-series, International Journal of Remote Sensing, 44:7, 2196-2215, DOI: [10.1080/01431161.2023.2197131](https://doi.org/10.1080/01431161.2023.2197131)

To link to this article: <https://doi.org/10.1080/01431161.2023.2197131>



Published online: 18 Apr 2023.



Submit your article to this journal 



View related articles 



View Crossmark data 



A deep convolutional neural network for burn progression mapping using Sentinel-1 SAR time-series

Ali Radman ^a, Reza Shah-Hosseini  ^a and Saeid Homayouni  ^b

^aRemote Sensing Department, School of Surveying and Geospatial Engineering, College of Engineering, University of Tehran, Tehran, Iran; ^bInstitut national de la recherche scientifique, Centre Eau Terre Environnement, Québec, QC, Canada

ABSTRACT

Forest fires burn various natural ecosystems worldwide and can harm the environment and human life. Accordingly, real-time monitoring of this phenomenon and early decision-making warning is vital. Active remote sensing systems, such as Synthetic Aperture Radar (SAR) sensors, provide an excellent opportunity for burn mapping because they can penetrate through clouds and smoke day and night. In this study, the potential of Sentinel-1 SAR data was investigated by deploying a deep convolutional neural network (CNN) based framework to map burn progression dynamically, in both supervised and transfer manners. Accordingly, an optimized deep architecture was designated to use SAR data features with high sensitivity to map the burned areas. The proposed method includes three main steps: 1) extraction of SAR indices, 2) training deep CNN model with a limited number of scenes and 3) assessing the transferability of the CNN for estimating burn progression for any unseen scene. Sentinel-1 SAR indices of log-ratio, radar burn difference (RBD), and difference of dual-polarization SAR vegetation index (Δ DPSVI) were obtained to be fed to the CNN. To validate the efficiency of the proposed approach, two fire events, i.e. the Derazno fire in Iran (2021) and the Rossomanno-Grottascura-Bellia fire in Italy (2017), were considered. For the scenes including training samples, the proposed method improved the overall accuracies (OAs) of classical machine learning techniques (i.e. SVM and RF) significantly (more than 4%). However, the improvement was minor when compared to a CNN using only log-ratio as the input channel (log-ratio CNN). For the scenes without training samples (unseen dates), the investigated transferred model performed substantially better (3% higher OA) compared to the other machine learning methods and the log-ratio CNN. This finding approves that the obtained SAR indices boost the transferability of the CNN model for burn progression mapping at unseen scenes.

ARTICLE HISTORY

Received 27 October 2022

Accepted 27 March 2023

KEYWORDS

Sentinel-1; SAR; burn mapping; radar indices; convolutional neural network; transfer model

1. Introduction

Wildfires affect the natural ecosystem and cause enormous damage to the environment. Over 50 million hectares worldwide are influenced by this phenomenon yearly (Lasaponara and Tucci 2019). In addition, long-term detriments threaten burned regions, including soil erosion,



air pollution and global climate change (Bernhard, Twele, and Gähler 2012; Gitas et al. 2012; Leblon, Bourgeau-Chavez, and San-Miguel-Ayanz 2012; de Luca, Silva, and Modica 2021). To avoid these harmful consequences, dynamic wildfire detection and monitoring are indispensable. Real-time mapping of fire progression can provide valuable early warning and decision-making information.

Satellite remote sensing data have allowed it to observe earth changes and wildfires with varied temporal and spatial resolutions. Numerous studies have utilized optical and multi-spectral satellite data for this purpose. Visible Infrared Imaging Radiometer Suite (VIIRS) and Moderate-resolution Imaging Spectroradiometer (MODIS) with low spatial and high temporal resolution have been used diversely (Schroeder et al. 2008; Maier and Russell-Smith 2012; Schroeder et al. 2014). On the other hand, the Landsat series and Sentinel-2 (S2) provide a higher spatial resolution for burned area mapping (Verhegghen et al. 2016; Quintano, Fernández-Manso, and Fernández-Manso 2018). However, all these datasets have limitations for real-time monitoring due to cloud cover (Crowley et al. 2019; Ban et al. 2020).

Synthetic Aperture Radar (SAR) active sensors can monitor earth observations in any weather condition, day or night. Accordingly, SAR data make it possible to map wildfires, owing to their constant ability to penetrate through clouds and smoke. Different SAR X-, C-, and L-bands' backscatter sensitivity and potential for burn detection are examined by Tanase et al. (2010), demonstrating their ability in this field. Sentinel-1 (S1) C-band SAR data have been investigated for burn area detection using varied classical methods, including thresholding, burn indices and supervised and unsupervised classification. Washaya, Balz, and Mohamadi (2018) deployed a threshold-based strategy and coherence map of S1 VV polarization for disaster monitoring. Engelbrecht et al. (2017) proposed a simple normalized difference α index (ND α) to map burn-scars using C-band SAR data, which uses the α parameter of H- α decomposition. Imperatore et al. (2017) and Lasaponara and Tucci (2019) utilized SAR backscatters together with unsupervised classification methods of seeded region growing (SRG) and ISODATA, respectively, to detect burn areas. de Luca, Silva, and Modica (2021) combine indices and segmentation methods for burn mapping. Several SAR indices and the grey-level co-occurrence matrix (GLCM) were considered SAR features. Eventually, the GLCM image size was reduced by applying principal component analysis (PCA), and the burn areas were detected through k-means clustering.

Deep learning (DL) based approaches have attracted researchers' attention in various fields of remote sensing, including land cover and land use classification (Huang, Zhao, and Song 2018; Memon et al. 2021), regression (Zhang et al. 2021; Boulila et al. 2021) as well as change detection (Asokan and Anitha 2019; Keshk and Yin 2020; Karim and van Zyl 2021). A wide range of deep methods have been investigated (Hinton, Osindero, and Teh 2006; Lange and Riedmiller 2010; Gong et al. 2017), while convolutional neural networks (CNNs) have emerged as the most promising ones. Thus far, several studies have deployed this learning algorithm alongside SAR operational data for burned area mapping. Zhang et al. (2019) presented an implicit radar convolutional burn index (RCBI) to detect burned regions. RCBI is based on S1 intensity and phase information of VV and VH polarizations. They demonstrated the applicability of SAR backscatter and coherency information for burn mapping with deep CNNs. On the other hand, Ban et al. (2020) illustrated that using only SAR backscatter information can provide sufficient information for wildfire detection. Accordingly, this data was obtained to monitor wildfire progression in real-time using a CNN framework.

This paper investigates the potential of S1 C-band SAR backscatter information for dynamic and real-time burn mapping. Therefore, we first extract different features from intensity data to fully consider the high potential of SAR data. Accordingly, log-ratio (for VV and VH), radar burn difference (RBD) (for VV and VH) and dual-polarization SAR vegetation index (DPSVI) are obtained to construct five input channels of the CNN for supervised classification of the area into the burn and unburn regions. The CNN would be learned using only one post-fire image (of each ascending and descending orbit). The burn map for other post-fire images would be generated without further training the model (by transferring the trained model). The main contribution and objectives of the current study are as follows:

- (1) Proposing five input channels for fully considering Sentinel-1 SAR dual-polarization features. Thus, log-ratio and RBD are extracted for both VV and VH polarizations, and alongside Δ DPSVI, the five input channels are prepared to be fed to the deep model.
- (2) Investigating an optimized CNN architecture to make the most out of the SAR extracted features and improve the burn area mapping accuracy.
- (3) Constructing a model for real-time and continuous monitoring of burn area progression using a transfer learning approach. So, the model is trained by only one post-fire image (of each orbit), and the burn map for the rest of the time series would be estimated using the transferred model.

2. Study areas and data

2.1. Study areas

The Derazno Fire occurred in Golestan Province, north of Iran, on 23 September 2021, and burned almost 200 ha of forests (Figure 1 (bottom-right)). Furthermore, it resulted in the injuries of 33 firefighters. The Derazno burned region is a Caspian Hyrcanian mixed forest that almost burned for 4 days. Oak, juniper trees and grasslands dominate Derazno area vegetation cover. It has a relatively high altitude of 2,600 m above sea surface and the highest mountain with 2,800 m altitude. One of the prominent features of the vegetation around the village of Derazno is the combination of forest and grasslands next to each other. Derazno's dense forests are covered with thyme, nettle, camomile, shrubs of medlar, barberry, wild apple, and pear. Wild animals such as boars and brown bears also live at high altitudes.

The second fire case study on 6 August 2017 was a large wildfire that burned approximately 3,851 ha in the Rossomanno-Grottascura-Bellia regional nature reserve, the central area of Sicily, south of Italy (de Luca, Silva, and Modica 2021) (Figure 1 (bottom-left)). This region has plateaus at around 800 m above sea level. Mediterranean forests, including genus Eucalyptus species and typical Mediterranean conifers, are the primary vegetation coverage of the territory (de Luca, Silva, and Modica 2021). This area is home to a wide range of animal species, including diverse bird species (i.e. buzzard and kestrel). Other animals, such as foxes and porcupines, live in this region.

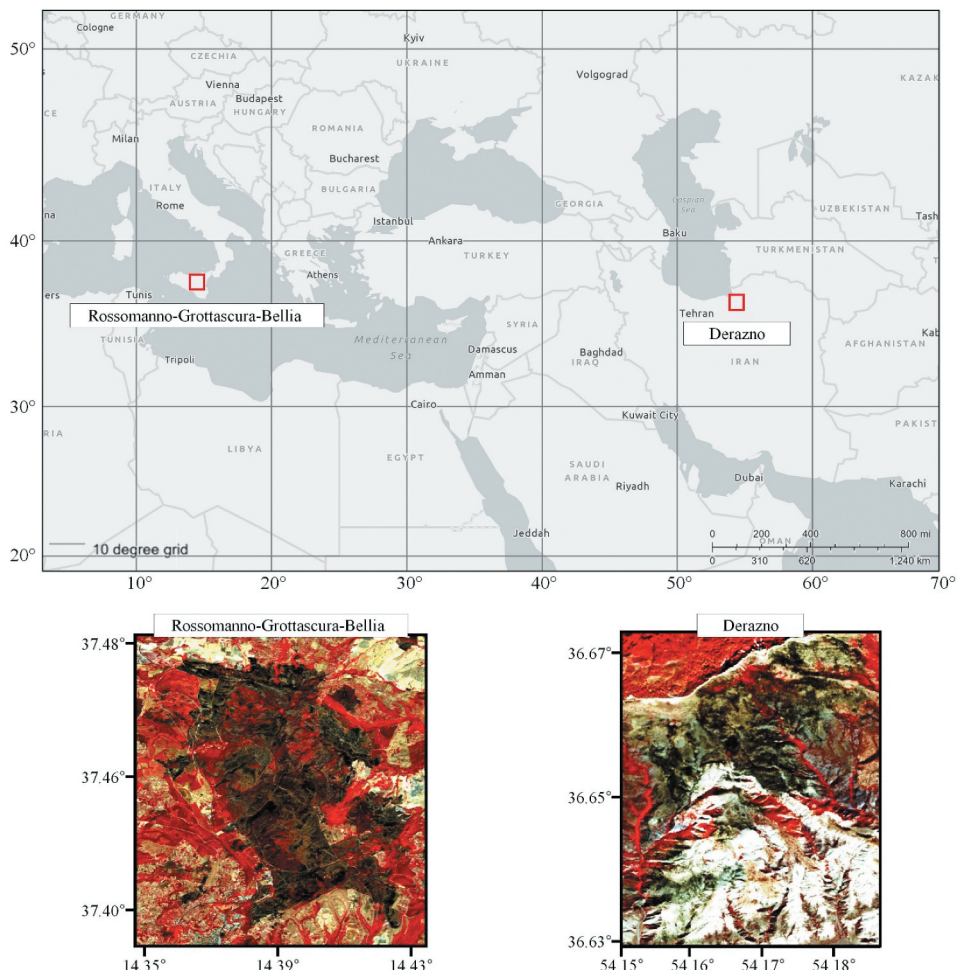


Figure 1. Study area: (top) location of case studies worldwide and in their countries (Italy and Iran). Bottom-left: Rossomanno-grottascura-bellia and bottom-right: Derazno post-fire Sentinel-2 images (RGB: NIR, green and blue pseudocolor images).

2.2. Remote-sensing data

2.2.1. SAR data

Sentinel-1 (S1), the first Copernicus mission, consists of twin satellites, S1-A and S1-B, that provide dual-polarization C-band SAR data with a 6-day temporal resolution. In the current study, the S1 level-1 ground range detected (GRD) product in interferometric wide swath (IW) mode was utilized through Google Earth Engine (GEE) platform (Gorelick et al. 2017). The acquired S1 dataset was first subjected to a terrain correction to reduce the noise level. Then, a refined Lee speckle filter with a 7×7 window size was applied (Lee, Grunes, and De Grandi 1999). This size was determined based on the speckle filter's ability to preserve desired characteristics with the least amount of spatial resolution loss in the context of burn mapping using S1 SAR data (Donezar et al. 2019). The temporal distribution of acquired S1 data for Derazno and Rossomanno-Grottascura-Bellia is presented in Table 1.

Table 1. Temporal distribution of acquired S1 images.

Derazno		Rossomanno-Grottascura-Bellia	
Orbit	Date	Orbit	Date
Descending	27 August 2021	Descending	24 July 2017
Ascending	2 September 2021	Ascending	24 July 2017
Descending	8 September 2021	Ascending	29 July 2017
Ascending	14 September 2021	Descending	30 July 2017
Descending	20 September 2021	Descending	5 August 2017
Ascending	26 September 2021	Ascending	5 August 2017
Descending	2 October 2021	Ascending	10 August 2017
Ascending	8 October 2021	Descending	11 August 2017
Descending	14 October 2021	Descending	17 August 2017
Ascending	20 October 2021	Ascending	17 August 2017
Descending	26 October 2021	Ascending	22 August 2017
		Descending	23 August 2017

2.2.2. Reference data

To validate the S1 burn maps, Sentinel-2 multispectral images were obtained from GEE for both case studies before and after the fire. The normalized burn ratio (NBR) index is a well-known remote sensing index used to generate reference data in similar studies due to its promising ability to detect burn areas (Donezar et al. 2019; Zhang et al. 2019; Ban et al. 2020; Philipp and Levick 2020; de Luca, Silva, and Modica 2021). Accordingly, ΔNBR is calculated by subtracting pre- and post-fire NBRs (Miller et al. 2009):

$$NBR = (NIR - SWIR_2) / (NIR + SWIR_2) \quad (1)$$

$$\Delta NBR = NBR_{\text{pre-fire}} - NBR_{\text{post-fire}} \quad (2)$$

where *NIR* and *SWIR*₂ are near-infrared (band-8A) bands and short-wave infrared (band-12) of the S2 dataset; eventually, the reference ground truth map was produced based on ΔNBR results and further enhanced by visual interpretation of pre- and post-fire pseudocolor RGB images (with *SWIR*₂, *NIR*, and *Red*). In other words, we utilized ΔNBR and a manual threshold to best fit the burned areas in each case as an initial step. Then, by manually removing false alarms and adding undetected burn regions to the initial map based on the pseudocolor images, the final product was generated (Figure 2). This final map is used as ground truth to evaluate burn maps estimated from the SAR dataset.

3. Proposed methodology

The current study aims to build an optimized model based on deep convolutional to fully use SAR intensity information for dynamically mapping the burn progression area. The main stages of the proposed approach are indicated in Figure 3. First, SAR indices, including log-ratio, RBD, and $\Delta DPSVI$, are extracted to achieve this goal. This process is performed by considering both ascending (ASC) and descending (DES) images separately, so for each orbit (ASC and DES), one of the pre-fire images is regarded as a master to calculate five channels for the remaining SAR images. As a result, the SAR indices are concatenated to construct a five channel time-series for each orbit. Then, the two series (ASC and DES) of SAR channels are combined to construct a united time series. For this purpose, each of the indices in the ASC and DES series are normalized by dividing them into standard deviation of the indices in the corresponding orbit

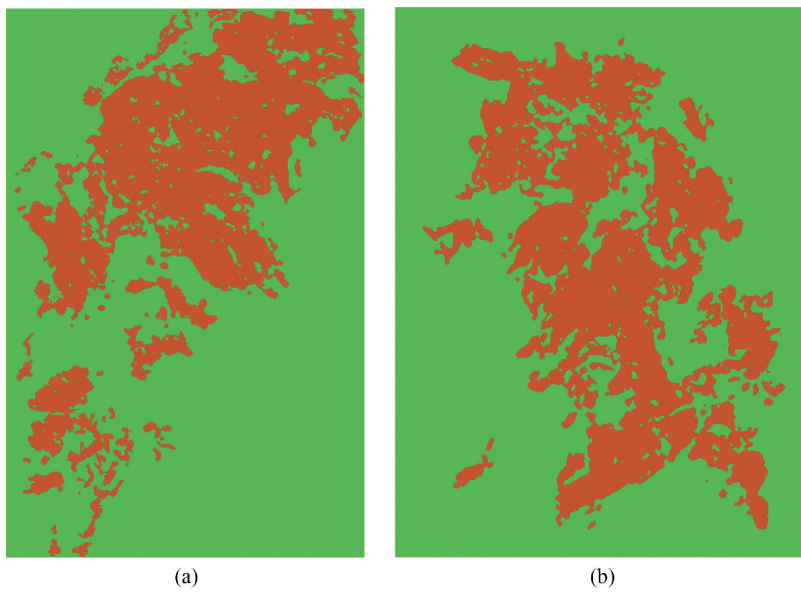


Figure 2. Produced burn map ground-truth for (a) Derazno fire, and (b) Rossomanno-Grottascura-Bellia fire.

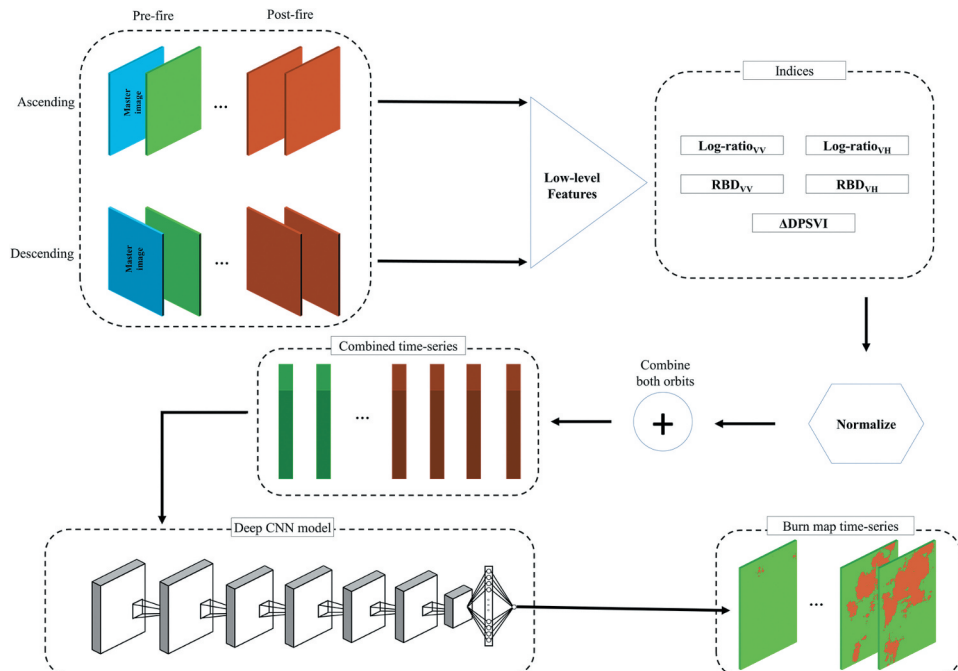


Figure 3. Workflow of the processing stages of the proposed approach for mapping burn progression time-series.

(ASC or DES). This combined time-series includes normalized images of both orbits, each of which is composed of five burn indices. In the last stage, the training samples of the combined time-series are fed to the proposed CNN for training the deep model and mapping the burn area progression of the time series.

3.1. Burn indices

Generally speaking, deep learning algorithms can automatically extract and learn high-level features from low-level characteristics (Touzi 2016). Extracting SAR characteristics that are more sensitive to burn areas would be beneficial to improve the learning process. As low-level features, three SAR indices of *log-ratio*, *RBD*, and Δ *DPSVI* are deployed; the first two can be computed for each VV and VH polarization, while the latter uses both. Log-ratio, also known as logarithmic radar burn ratio (*LogRBR*), is the most common SAR index and enhances the *RBR* by scaling it with the logarithm function. *Log-ratio* and *RBD* indices are represented as follows:

$$\text{log-ratio}^{XY} = 10 \log_{10} (I_{\text{post-fire}}^{XY} / I_{\text{pre-fire}}^{XY}) \quad (3)$$

$$\text{RBD}^{XY} = I_{\text{post-fire}}^{XY} - I_{\text{pre-fire}}^{XY} \quad (4)$$

where $I_{\text{post-fire}}^{XY}$ and $I_{\text{pre-fire}}^{XY}$ are SAR intensities of XY (VV or VH) polarization of the post-fire and pre-fire (master image), respectively. Δ *DPSVI* is the post- and pre-fire differential of the dual-polarization SAR vegetation index, which can be calculated by the following equations (Periasamy 2018).

$$\text{DPSVI} = (I^{\text{VW}} + I^{\text{VH}}) / I^{\text{VW}} \quad (5)$$

$$\Delta\text{DPSVI} = \text{DPSVI}_{\text{post-fire}} - \text{DPSVI}_{\text{pre-fire}} \quad (6)$$

Eventually, five channels of *log-ratio*^{VV}, *log-ratio*^{VH}, *RBD*^{VV}, *RBD*^{VH}, and Δ *DPSVI* are obtained to indicate SAR characteristics.

3.2. Convolutional neural network

This study uses a CNN to produce burn maps based on five normalized indices as input channels. The proposed architecture of the deep model is presented in Figure 4 and Table 2. Each layer contains a convolutional operation, followed by batch normalization, max-pooling (pooling size and stride of 2) and ReLu non-linear activation function (Krizhevsky, Sutskever, and Hinton 2012).

Convolutional layers use the feature extraction ability of kernels to obtain low- and high-level features over initial and deeper layers, respectively. The output of each convolutional layer is represented as follows:

$$H^l = h(w^l * H^{l-1} + b^l) \quad (7)$$

where H^l and H^{l-1} indicate the output of l^{th} and $(l-1)^{\text{th}}$ layers. (*) denotes the convolutional operation. w and b are weights and biases of the l^{th} layer, respectively. The third convolutional layer is followed by two fully connected (FC) layers and a sigmoid activation

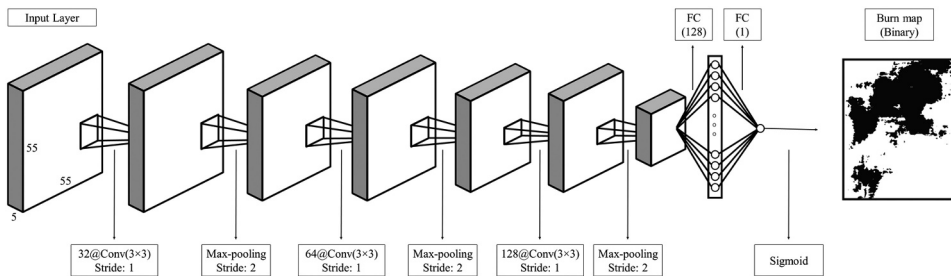


Figure 4. The proposed deep architecture for burn mapping.

Table 2. The architecture of the CNN model.

Layer	Operations
Input layer (size)	Input size $\times 55 \times 55 \times 5$
Layer 1	$32 @ 3 \times 3$ Conv + BN + Maxpool + ReLu
Layer 2	$64 @ 3 \times 3$ Conv + BN + Maxpool + ReLu
Layer 3	$128 @ 3 \times 3$ Conv + BN + Maxpool + ReLu
FC layer	$128 @ FC$ Encoder + BN + ReLu
Output layer	$1 @ FC$ Encoder + Sigmoid

function to generate a burn confidence map. Furthermore, a 0.5 dropout follows the last layer to reduce the overfitting effect.

To avoid overfitting issue, the entire network is trained using a cross-entropy loss function with an additional L2-norm regularization term (0.001). The training is implemented by minimizing the loss function with an Adam optimizer (Kingma and Jimmy 2014). The hyperparameters and other settings of the proposed model are adjusted over an experimental grid search. In the preparation stage of the CNN input data, a relatively large patch size of 55×55 is adapted to use the neighbourhood potential of convolutional layers. Accordingly, fixed-shaped $55 \times 55 \times 5$ cubic patches are the inputs of the network. After passing through the last layer activation function (sigmoid), a single scalar in the range of 0 to 1 estimates the burn confidence. A batch size of 200 and a learning rate (LR) of 0.0001 were investigated for training the model over 30 training epochs. A momentum of 0.9 is used for batch normalization.

3.3. State-of-the-art methods

To evaluate the proposed approach comprehensively, the results are compared to multiple state-of-the-art methods, including a support vector machine (SVM), random forest (RF), and a two-channel CNN (log-ratio CNN) with only considering log-ratio information, similar to Ban et al. (2020).

Vapnik (1999) developed the SVM algorithm, which has gained extensive attention in remote sensing classification studies (Chen, Zhao, and Lin 2014; Marcinkowska et al. 2014). This method works based on finding the optimum hyperplane to maximize the margin between classes. In this study, we obtained the radial basis function (RBF), one of the most successful SVM kernels in remote sensing applications (Mountrakis, Jungho, and Ogole 2011; Sheykhmousa et al. 2020).

RF classification is an ensemble of independent tree classifiers with the highest voted tree class being considered as the assigned class (Breiman 2001). The overfitting problem does not significantly affect this method (Raczko and Zagajewski 2017). The two primary parameters of RF are the number of decision trees and the number of randomly selected features. Since RF is not a particularly complex algorithm, adding more trees can increase accuracy without considerably increasing computing costs (Guan et al. 2013). Five hundred trees were used in this study because it was determined to be the ideal quantity in various works (Belgiu and Drăguț 2016; Sheykhmousa et al. 2020). The number of input features is adjusted to the square root of the number of input features (Sheykhmousa et al. 2020).

To evaluate the impact of the five input channels (SAR indices) on the performance of the proposed approach, we compared it to a similar method using alternative input channels. Log-ratio is the most common SAR intensity index that has been used successfully for burn mapping (Lasaponara and Tucci 2019; Ban et al. 2020). Accordingly, we use a two-input channel CNN model (log-ratio CNN) with a similar architecture to the proposed method that utilizes $\text{log-ratio}^{\text{VV}}$ and $\text{log-ratio}^{\text{VH}}$ as inputs (instead of the five indices of the proposed approach).

3.4. Evaluation metrics

To evaluate the proposed method's performance for burn area mapping, four metrics, including overall accuracy (OA), precision (P), recall (R), and F_1 -score (F_1), are deployed. After classification, the generated burn map and the reference map are compared, and the following evaluation metrics were calculated:

$$\text{OA} = (\text{TP} + \text{TN}) / (\text{TP} + \text{FP} + \text{FN} + \text{TN}) \quad (8)$$

$$\text{P} = \text{TP} / (\text{TP} + \text{FP}) \quad (9)$$

$$\text{R} = \text{TP} / (\text{TP} + \text{FN}) \quad (10)$$

$$\text{F}_1 = 2 \times (\text{P} \times \text{R}) / (\text{P} + \text{R}) \quad (11)$$

These metrics are defined based on confusion matrix parameters. True positive (TP) and false positive (FN) present samples that correctly and incorrectly estimated positive (burn) labels, while true negative (TN) and false negative (FP) are the correctly and incorrectly classified negative (unburn) labelled samples.

4. Experimental results

The proposed method is implanted for two cases of Derazno and Rossomanno-Grottascura-Bellia. For each case study, the results are presented separately, visually and statistically, and compared to state-of-the-art techniques.

In burn mapping studies, the ground truth data might not be available due to the presence of clouds and smoke (Crowley et al. 2019; Ban et al. 2020). Therefore, supervised learning of learning-based classification approaches might not be a viable strategy. To demonstrate the applicability of the proposed approach to overcome this problem, we

analyse its transferability for mapping burned areas on unseen dates. Each of the case studies includes four post-fire images, of which two are considered for supervised training. The remaining images (i.e. pre-fire, during burn progression and the other two post-fire images) are used to assess the effectiveness of the transferred models.

4.1. Data preparation

Each image in the time-series contains 146,466 and 194,691 samples for the Derazno and Rossomanno-Grottascura-Bellia regions, respectively. The supervised training process is performed on two post-fire images for each case study, with the remaining images containing only test samples that are considered to represent transfer learning. Accordingly, 20000 training samples (10,000 samples per image) and 2,000 validation samples (1,000 samples per image) are randomly selected for the training stage, with the remaining samples being used for testing. Table 3 displays the details of the supervised training (with two post-fire images).

4.2. Derazno fire

Results of each processing stage and different burn mapping methods of the Derazno fire time series are shown in Figure 5. First, the extracted features from the log-ratio, RBD, and ΔDPSVI indices are depicted. To illustrate both log-ratio and RBD polarizations, red and blue (purple) show VH polarization, and green presents VV. Then, the burn confidence of the proposed CNN models is presented, followed by its corresponding burn map time series. It should be noted that only the seventh and eighth steps (10–14 (DES) and 10–20 (ASC)) are classified as supervised (using training samples).

Regarding the input channel feature maps, the VH (purple) log-ratio channel seems to contain more burn information than VV (green). In contrast, the impact of burn is more evident in the VV band of RBD (green) than in VH. RBD^{VH} and $\Delta DPSVI$ decrease in burned areas, while the other three channels, i.e. RBD^{VV} and log-ratio channels, increase over those regions. Although several enhancements (including a refined LEE speckle filter) were applied to the S1 SAR images, the input channels are still affected by noise. To mitigate this issue, a relatively large window with a patch size of 55×55 was deployed for the CNN model. The network burn confidence time series presents the effect of burned regions with a high correlation to real changes. The burn maps are generated by applying a global Otsu threshold to the burn confidence for the whole time series. The generated post-fire burn maps have almost detected burned regions (in the reference S2 image).

Table 3. Information about the number of samples for the supervised learning stage (scenes containing training data).

Case study	Total samples	Training		Validation		Test	
		Sample number	Ratio (%)	Sample number	Ratio (%)	Sample number	Ratio (%)
Derazno	292,932	20,000	6.83	2,000	0.683	270,932	92.49
Rossomanno-Grottascura-Bellia	389,382	20,000	5.14	2,000	0.514	367,382	94.35

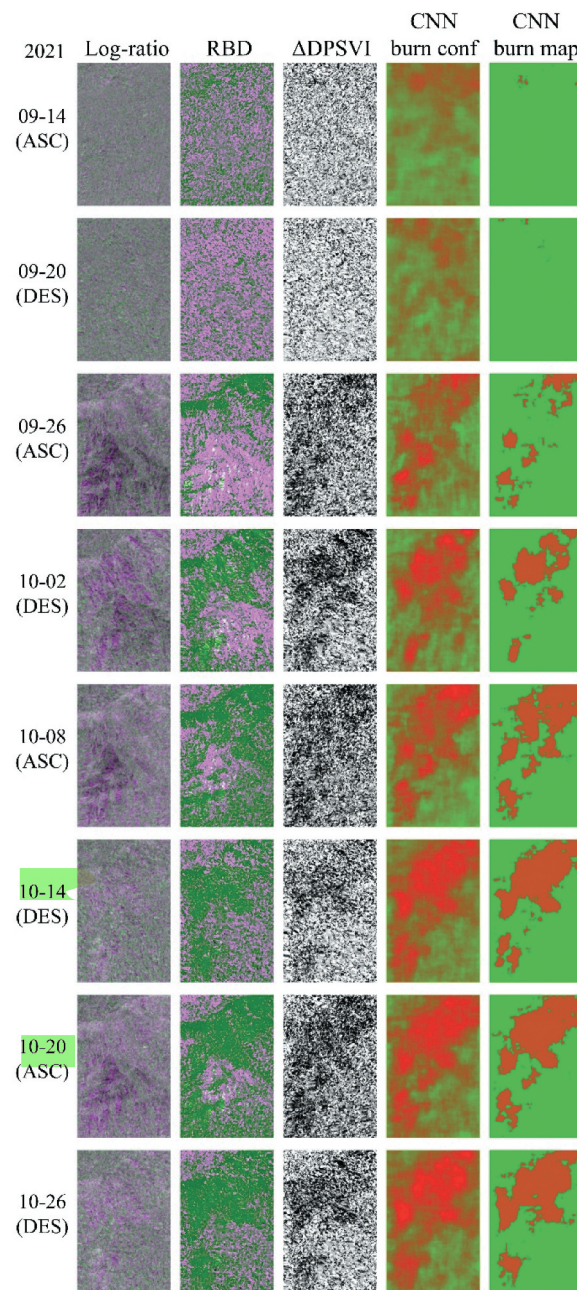


Figure 5. Time-series results of Derazno fire. First two columns present log-ratio and RBD pseudocolor images (VH-VV-VH polarizations). The third column is Δ DPSVI. The fourth column indicates investigated CNN burn confidence map, followed by the binary burn map in the last column.

Table 4. Accuracy of estimated post-fire burn maps of Derazno fire (* indicates the images with training samples).

Burn map	P	R	F1	OA
ASC (10–08)	76.29	77.33	76.82	84.94
DES (10–14)*	81.66	83.56	82.53	88.70
ASC (10–20)*	84.54	82.71	83.58	89.16
DES (10–26)	75.51	75.12	75.29	83.79

4.2.1. Quantitative analysis

The post-fire maps are evaluated quantitatively compared to the reference S2 burn map (**Table 4**). It is evident from the table that burn maps of images with training samples have better accuracies. These burn maps achieved above 81% P, R, and F₁. Moreover, 88.71% and 89.15% OAs illustrate the overall capability of the method for burn mapping. On the other hand, the burn maps of the transferred model achieved acceptable accuracies above 75% P, R, and F₁. The above 83% OAs prove the transferability of the model for dynamic burn progression mapping.

4.2.2. Comparison with other methods

To comprehensively evaluate the proposed framework, the results are compared to SVM and RF traditional models, as well as a CNN, using only log-ratio as input (log-ratio CNN) to indicate the impact of the feature extraction step (five input channels). The post-fire burn maps are shown in [Figure 6](#).

In [Table 5](#), the performance of the models is compared for scenes with training samples (or supervised) and the scenes that are estimated using the transferred model (burn maps without training samples).

4.3. Rossomanno-Grottascura-Bellia fire

The results of the proposed method for the Rossomanno-Grottascura-Bellia fire are represented in [Figure 7](#). Log-ratio, RBD, and ΔDPSVI indices are shown in the first three columns, using pseudocolor image log-ratio and RBD for VH (red and blue bands) and VV polarizations (green band). The proposed CNN-based burn confidence time series and the final burn map follow the burn indices. For the training of the model, training samples are only considered from the seventh and ninth images (08–17 (DES) and 08–22 (ASC)) of the time-series. Then, the trained model classifies the whole time series.

Both polarizations are sensitive to burned areas regarding the log-ratio, as shown by an increment in the index intensity (light areas in [Figure 7](#), first column). However, VH seems to have a better correlation with burned areas. Over the burned regions, there is a rise in VV and a decline in the RBD index's VH polarizations. The fire effect also led to ΔDPSVI reduction. The burn confidence time series of the CNN classifier seems to have a reasonable correlation with the indices and the burned area. Applying the Otsu threshold to the burn confidence produces burn map time series. Post-fire burn maps detect burned areas similar to the reference burn map. The post-fire burn maps are considered for further statistical assessments.

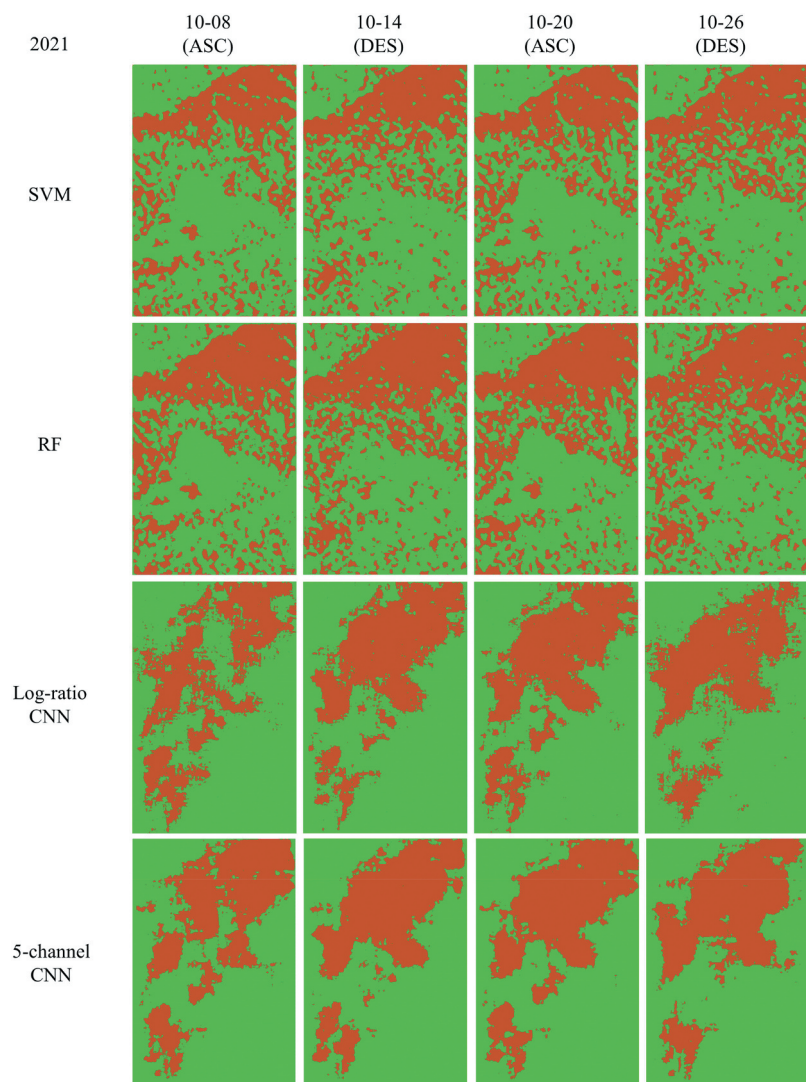


Figure 6. Comparison of produced post-fire burn maps (Derazno fire).

Table 5. Accuracy of the proposed CNN compared to other methods (Derazno fire).

Method	<i>P</i>		<i>R</i>		<i>F1</i>		OA	
	Supervised	Transferred	Supervised	Transferred	Supervised	Transferred	Supervised	Transferred
SVM	58.4	57.33	54.42	52.41	56.34	54.68	70.33	69.07
RF	70.66	64.40	55.19	51.02	61.97	56.96	71.59	68.04
Log-ratio CNN	81.93	68.73	80.78	69.15	81.32	68.95	87.68	79.74
Proposed CNN	83.06	75.85	83.11	76.23	83.13	76.02	88.92	84.33

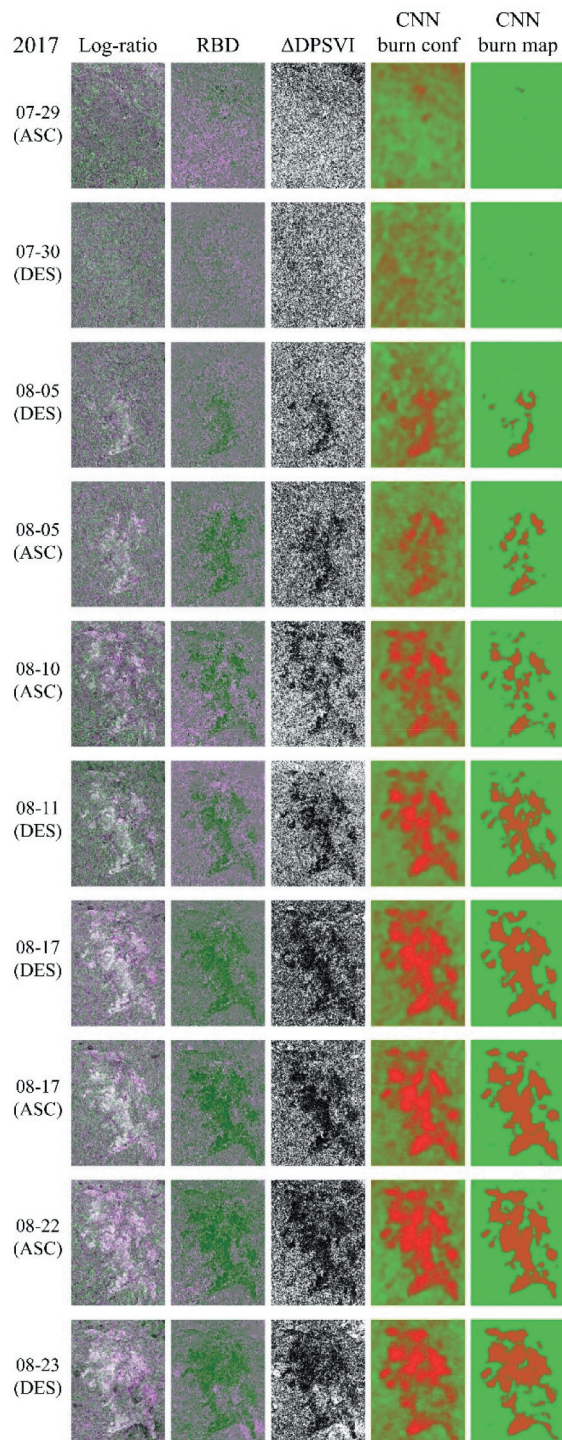


Figure 7. Time series results of Rossomanno-Grottascura-Bellia fire. First two columns present log-ratio and RBD pseudocolor images (VH-VV-VH polarizations). The third column is Δ DPSVI. The fourth column indicates investigated CNN burn confidence map, followed by the binary burn map in the last column.

Table 6. Accuracy of the estimated post-fire burn maps of Rossomanno-Grottascura-Bellia fire (* indicates the images with training samples).

Burn map	P	R	F1	OA
DES (8-17)*	79.15	80.22	79.63	87.31
ASC (8-17)	77.22	76.07	76.65	85.26
ASC (8-22)*	78.63	81.94	80.26	87.89
DES (8-23)	73.07	73.25	73.19	83.20

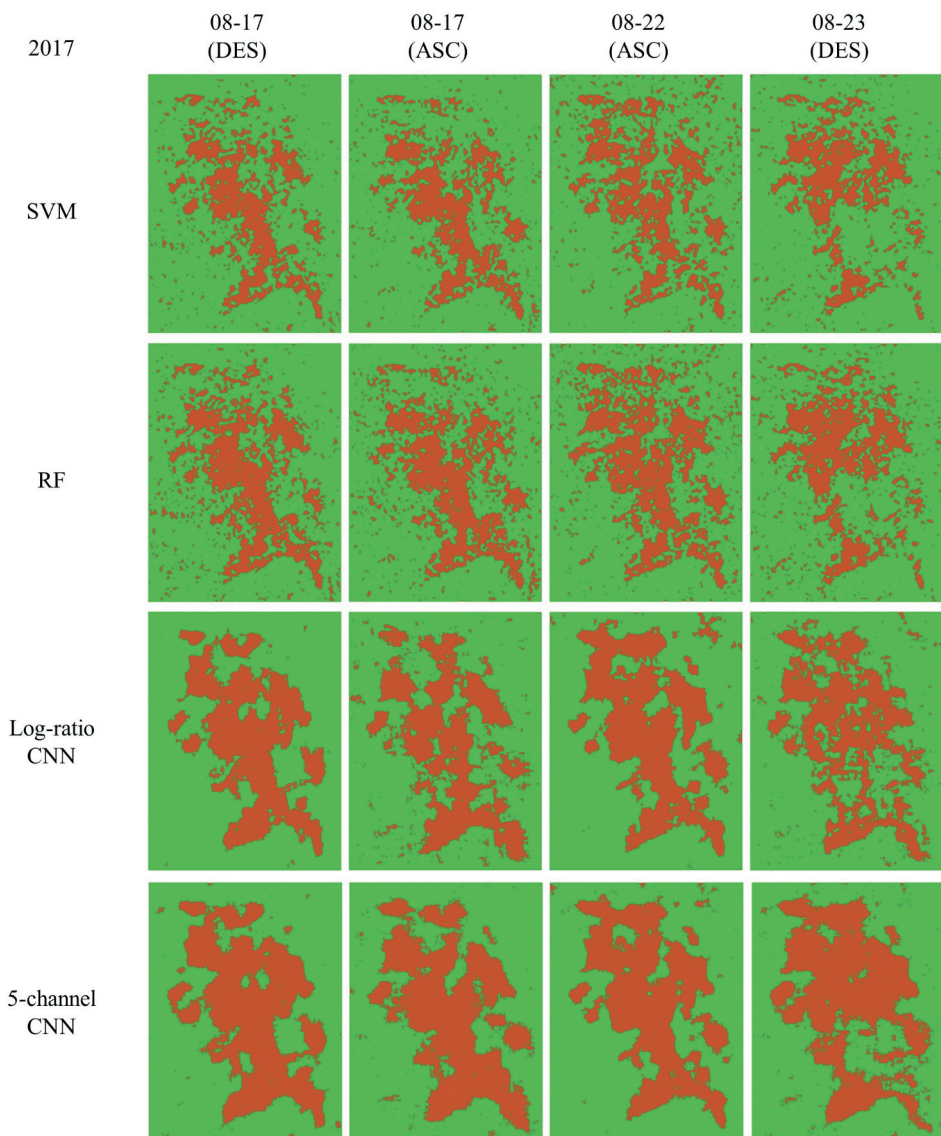


Figure 8. Comparison of produced post-fire burn maps (Rossomanno-Grottascura-Bellia fire).

Table 7. Accuracy of the proposed CNN compared to other methods (Rossomanno-Grottascura-Bellia fire).

Method	P		R		F1		OA	
	Supervised	Transferred	Supervised	Transferred	Supervised	Transferred	Supervised	Transferred
SVM	63.24	58.92	76.03	77.37	68.95	66.86	82.15	81.70
RF	72.05	63.54	73.35	70.28	72.63	66.68	82.97	80.14
Log-ratio CNN	80.75	71.31	79.37	69.43	80.00	70.35	87.33	81.13
Proposed CNN	78.88	75.16	81.06	74.64	79.99	74.91	87.62	84.22

4.3.1. Quantitative analysis

Table 6 represents the accuracy of the estimated post-fire burn maps. The burn maps that contain training samples reached above 78% P, R, and F₁ and approximately 87% OA, while these statistics are lower for the generated burn maps with a transferred model. However, OAs of 85.23% and 83.18% indicate the potential of the transferred model for dynamic burned area detection.

4.3.2. Comparison with other methods

Figure 8 visually compares the proposed CNN, SVM, RF, and log-ratio CNN post-fire burn maps. In general, compared to the Derazno case, all techniques have produced burn maps that are closer to ground truth data. However, the predicted maps by SVM and RF are still noisy and contain undetected regions.

Table 7 compares the accuracies of post-fire burn maps. The comparison is conducted for images with training samples (supervised) and without training samples (transferred).

5. Discussion

This section discusses and analyzes both visual and statistical results. Accordingly, the effectiveness of the proposed approach is discussed for both case studies in comparison to state-of-the-art methods.

5.1. Visual analyzes

In Derazno case (Figure 6), the machine learning techniques (SVM and RF) resulted in noisy maps with many false alarms and undetected burn regions. Both deep CNN approaches led to almost similar maps for supervised scenes. Meanwhile, the CNN model with only log-ratio as input has left several undetected burn regions for transferred samples.

For the Rossomanno-Grottascura-Bellia (Figure 8), the deep models' burn maps are remarkably close, even for transferred scenes. Nevertheless, the proposed five-channel technique has a lower noise level and a slightly stronger capacity to identify burned regions in the transferred samples.

In general, the traditional machine learning methods had weak performance compared to CNN models. When using deep CNN, the model with five input channel indices had a slightly lower noise level and higher sensitivity to burned areas compared to the model with only log-ratio inputs.

5.2. Statistical analyzes

The accuracies of the transferred models are considerably lower for all the methods in the Derzno case ([Table 4](#)). The SVM and RF resulted in poor accuracies compared to the CNN models. Their results have similar OAs and better performance of random forest over supervised and conversely. The log-ratio CNN has almost similar accuracies to the proposed method over images with training samples (about 1% lower OA). At the same time, its transferred model accuracy falls significantly (about 5% lower OA). It demonstrates that five input channels improve the transferability of the CNN model. The ability of the proposed model is helpful for the dynamic mapping of fire progression.

For the Rossomanno-Grottascura-Bellia case ([Table 6](#)), the transferred model's accuracy is relatively less than the supervised one for all the methods. Overall, SVM and RF have poor precision (P), meaning many burn areas have not been detected. In contrast, their higher recall shows that they have less false burn detection. Accordingly, their high OAs (above 80%) is due to good unburned class detection, while they failed to detect burn regions. Log-ratio CNN performance has great potential for supervised mapping of burn areas by reaching P and F1 of 80.77% and 80.01%, slightly more than the proposed method. However, the performance of its transferred model is notably (3% less OA) weaker. This indicates the considerable impact of the proposed five input channels on the transferability of the CNN model for dynamic fire progression mapping.

Overall, the effectiveness of the traditional machine learning techniques (SVM and RF) varies depending on the case, although they are consistently inferior when compared to CNN models. CNN models showed impressive potential for identifying burned regions even when only using Log-ratio as the model's input. Meanwhile, for burn progression mapping of unseen dates with transferred models, the proposed approach with five input channels significantly improves the network's performance, i.e. more than 5% and 3% improvement in all utilized accuracy parameters (P, R, F1, and OA) for Derazno and Rossomanno-Grottascura-Bellia, respectively.

6. Conclusion

This study proposes a dynamic burn mapping method that obtains a high S1 SAR back-scattering information potential. Thus, both VV and VH polarizations of S1 images are considered to obtain log-ratio, RBD, and Δ DPSVI. Accordingly, these features are fed to an optimized CNN for classifying burn progression. This network is trained using one sample image (of each orbit), which then produces a burn map at any unseen time.

Experimental results of the presented approach proved its satisfying ability for burn mapping, which improved the OA of classical methods by 15% and 3% for Derazno and Rossomanno-Grottascura-Bellia cases. It also demonstrated that the extracted SAR channels could slightly enhance CNN results compared to a simple log ratio.

In addition, the investigated five-channel CNN model makes dynamic mapping of fire progression possible. It achieved above 80% OAs for both case studies in estimating real-time burn maps. While the log-ratio CNN model showed almost identical accuracy to the suggested framework over images with training samples, its accuracy over transferred burned maps was more than 3% inferior. This issue demonstrates the impact of the considered SAR indices on the transferability of the CNN model. Accordingly, the

proposed framework provides a transfer learning approach that can be used for a rapid and dynamic map of fire progression on small and large scales.

Disclosure statement

No potential conflict of interest was reported by the authors.

ORCID

Ali Radman  <http://orcid.org/0000-0002-7030-8794>
 Reza Shah-Hosseini  <http://orcid.org/0000-0002-7552-5392>
 Saeid Homayouni  <http://orcid.org/0000-0002-0214-5356>

References

- Asokan, A., and J. Anitha. 2019. "Change Detection Techniques for Remote Sensing Applications: A Survey." *Earth Science Informatics* 12 (2): 143–160. doi:[10.1007/s12145-019-00380-5](https://doi.org/10.1007/s12145-019-00380-5).
- Ban, Y., P. Zhang, A. Nascetti, A. R. Bevington, and M. A. Wulder. 2020. "Near Real-Time Wildfire Progression Monitoring with Sentinel-1 SAR Time Series and Deep Learning." *Scientific Reports* 10 (1): 1–15. doi:[10.1038/s41598-019-56967-x](https://doi.org/10.1038/s41598-019-56967-x).
- Belgiu, M., and L. Drăguț. 2016. "Random Forest in Remote Sensing: A Review of Applications and Future Directions." *ISPRS Journal of Photogrammetry Remote Sensing* 114: 24–31. doi:[10.1016/j.isprsjprs.2016.01.011](https://doi.org/10.1016/j.isprsjprs.2016.01.011).
- Bernhard, E. -M., A. Twele, and M. Gähler. 2012. "Burnt Area Mapping in the European-Mediterranean: SAR Backscatter Change Analysis and Synergistic Use of Optical and SAR Data." 2012 IEEE International Geoscience and Remote Sensing Symposium, Munich, Germany. 2141–2143. doi:[10.1109/IGARSS.2012.6351080](https://doi.org/10.1109/IGARSS.2012.6351080).
- Boulila, W., H. Ghadorh, M. Ahmed Khan, F. Ahmed, and J. Ahmad. 2021. "A Novel CNN-LSTM-Based Approach to Predict Urban Expansion." *Ecological Informatics* 64: 101325. doi:[10.1016/j.ecoinf.2021.101325](https://doi.org/10.1016/j.ecoinf.2021.101325).
- Breiman, L. 2001. "Random Forests." *Machine Learning* 45: 5–32. doi:[10.1023/A:1010933404324](https://doi.org/10.1023/A:1010933404324).
- Chen, Y., X. Zhao, and Z. Lin. 2014. "Optimizing Subspace SVM Ensemble for Hyperspectral Imagery Classification." *IEEE Journal of Selected Topics in Applied Earth Observations Remote Sensing* 7 (4): 1295–1305. doi:[10.1109/JSTARS.2014.2307356](https://doi.org/10.1109/JSTARS.2014.2307356).
- Crowley, M. A., J. A. Cardille, J. C. White, and M. A. Wulder. 2019. "Multi-Sensor, Multi-Scale, Bayesian Data Synthesis for Mapping Within-Year Wildfire Progression." *Remote Sensing Letters* 10 (3): 302–311. doi:[10.1080/2150704X.2018.1536300](https://doi.org/10.1080/2150704X.2018.1536300).
- de Luca, G., J. M. Silva, and G. Modica. 2021. "A Workflow Based on Sentinel-1 SAR Data and Open-Source Algorithms for Unsupervised Burned Area Detection in Mediterranean Ecosystems." *GI/Science & Remote Sensing* 58: 1–26. doi:[10.1080/15481603.2021.1907896](https://doi.org/10.1080/15481603.2021.1907896).
- Donezar, U., T. De Blas, A. Larrañaga, F. Ros, L. Albizua, A. Steel, and M. Broglia. 2019. "Applicability of the Multitemporal Coherence Approach to Sentinel-1 for the Detection and Delineation of Burnt Areas in the Context of the Copernicus Emergency Management Service." *Remote Sensing* 11 (22): 2607. doi:[10.3390/rs11222607](https://doi.org/10.3390/rs11222607).
- Engelbrecht, J., A. Theron, L. Vhengani, and J. Kemp. 2017. "A Simple Normalized Difference Approach to Burnt Area Mapping Using Multi-Polarisation C-Band SAR." *Remote Sensing* 9 (8): 764. doi:[10.3390/rs9080764](https://doi.org/10.3390/rs9080764).
- Gitas, I., G. Mitri, S. Veraverbeke, and A. Polychronaki. 2012. "Advances in Remote Sensing of Post-Fire Vegetation Recovery Monitoring—A Review." *Remote Sensing of Biomass-Principles and Applications* 1: 334.

- Gong, M., X. Niu, P. Zhang, and L. Zhetao. 2017. "Generative Adversarial Networks for Change Detection in Multispectral Imagery." *IEEE Geoscience and Remote Sensing Letters* 14 (12): 2310–2314. doi:[10.1109/LGRS.2017.2762694](https://doi.org/10.1109/LGRS.2017.2762694).
- Gorelick, N., M. Hancher, M. Dixon, S. Ilyushchenko, D. Thau, and R. Moore. 2017. "Google Earth Engine: Planetary-Scale Geospatial Analysis for Everyone." *Remote Sensing of Environment* 202: 18–27. doi:[10.1016/j.rse.2017.06.031](https://doi.org/10.1016/j.rse.2017.06.031).
- Guan, H., L. Jonathan, M. Chapman, F. Deng, J. Zheng, and X. Yang. 2013. "Integration of Orthoimagery and Lidar Data for Object-Based Urban Thematic Mapping Using Random Forests." *International Journal of Remote Sensing* 34 (14): 5166–5186. doi:[10.1080/01431161.2013.788261](https://doi.org/10.1080/01431161.2013.788261).
- Hinton, G. E., S. Osindero, and Y. W. Teh. 2006. "A Fast Learning Algorithm for Deep Belief Nets." *Neural Computation* 18 (7): 1527–1554. doi:[10.1162/neco.2006.18.7.1527](https://doi.org/10.1162/neco.2006.18.7.1527).
- Huang, B., B. Zhao, and Y. Song. 2018. "Urban Land-Use Mapping Using a Deep Convolutional Neural Network with High Spatial Resolution Multispectral Remote Sensing Imagery." *Remote Sensing of Environment* 214: 73–86. doi:[10.1016/j.rse.2018.04.050](https://doi.org/10.1016/j.rse.2018.04.050).
- Imperatore, P., R. Azar, F. Calo, D. Stroppiana, P. Alessandro Brivio, R. Lanari, and A. Pepe. 2017. "Effect of the Vegetation Fire on Backscattering: An Investigation Based on Sentinel-1 Observations." *IEEE Journal of Selected Topics in Applied Earth Observations and Remote Sensing* 10 (10): 4478–4492. doi:[10.1109/JSTARS.2017.2717039](https://doi.org/10.1109/JSTARS.2017.2717039).
- Karim, Z., and T. L. van Zyl. 2021. "Deep/Transfer Learning with Feature Space Ensemble Networks (FeatSpaceensnets) and Average Ensemble Networks (AvgEnsnets) for Change Detection Using DInSar Sentinel-1 and Optical Sentinel-2 Satellite Data Fusion." *Remote Sensing* 13 (21): 4394. doi:[10.3390/rs13214394](https://doi.org/10.3390/rs13214394).
- Keshk, H. M., and X. C. Yin. 2020. "Change Detection in SAR Images Based on Deep Learning." *International Journal of Aeronautical and Space Sciences* 21 (2): 549–559. doi:[10.1007/s42405-019-0022-0](https://doi.org/10.1007/s42405-019-0022-0).
- Kingma, D. P., and B. Jimmy. 2014. "Adam: A Method for Stochastic Optimization." *arXiv preprint arXiv:1412.6980*.
- Krizhevsky, A., I. Sutskever, and G. E. Hinton. 2012. "Imagenet Classification with Deep Convolutional Neural Networks." *Advances in Neural Information Processing Systems* 25: 1097–1105.
- Lange, S., and M. Riedmiller. 2010. "Deep Auto-Encoder Neural Networks in Reinforcement Learning." The 2010 International Joint Conference on Neural Networks (IJCNN), Barcelona, Spain, 1–8. doi:[10.1109/IJCNN.2010.5596468](https://doi.org/10.1109/IJCNN.2010.5596468).
- Lasaponara, R., and B. Tucci. 2019. "Identification of Burned Areas and Severity Using SAR Sentinel-1." *IEEE Geoscience and Remote Sensing Letters* 16 (6): 917–921. doi:[10.1109/LGRS.2018.2888641](https://doi.org/10.1109/LGRS.2018.2888641).
- Leblon, B., L. Bourgeau-Chavez, and J. San-Miguel-Ayanz. 2012. "Use of Remote Sensing in Wildfire Management." *Sustainable Development-Authoritative and Leading Edge Content for Environmental Management*, 55–82. InTech. doi:[10.5772/45829](https://doi.org/10.5772/45829).
- Lee, J. S., M. R. Grunes, and G. De Grandi. 1999. "Polarimetric SAR Speckle Filtering and Its Implication for Classification." *IEEE Transactions on Geoscience and Remote Sensing* 37 (5): 2363–2373. doi:[10.1109/36.789635](https://doi.org/10.1109/36.789635).
- Maier, S. W., and J. Russell-Smith. 2012. "Measuring and Monitoring of Contemporary Fire Regimes in Australia Using Satellite Remote Sensing." *Flammable Australia: Fire Regimes, Biodiversity and Ecosystems in a Changing World*, 79–95. CSIRO Publishing. <http://www.publish.csiro.au/book/6836/#contents>
- Marcinkowska, A., B. Zagajewski, A. Ochtyra, A. Jarocińska, E. Raczkó, L. Kupková, P. Stych, and K. Meuleman. 2014. "Mapping Vegetation Communities of the Karkonosze National Park Using APEX Hyperspectral Data and Support Vector Machines." *Miscellanea Geographica* 18 (2): 23–29. doi:[10.2478/mgrsd-2014-0007](https://doi.org/10.2478/mgrsd-2014-0007).
- Memon, N., H. Parikh, S. B. Patel, D. Patel, and V. D. Patel. 2021. "Automatic Land Cover Classification of Multi-Resolution Dualpol Data Using Convolutional Neural Network (CNN)." *Remote Sensing Applications: Society and Environment* 22: 100491. doi:[10.1016/j.rsase.2021.100491](https://doi.org/10.1016/j.rsase.2021.100491).

- Miller, J. D., E. E. Knapp, C. H. Key, C. N. Skinner, C. J. Isbell, R. Max Creasy, and J. W. Sherlock. 2009. "Calibration and Validation of the Relative Differenced Normalized Burn Ratio (RdNbr) to Three Measures of Fire Severity in the Sierra Nevada and Klamath Mountains, California, USA." *Remote Sensing of Environment* 113 (3): 645–656. doi:[10.1016/j.rse.2008.11.009](https://doi.org/10.1016/j.rse.2008.11.009).
- Mountrakis, G., I. Jungho, and C. Ogole. 2011. "Support Vector Machines in Remote Sensing: A Review." *ISPRS Journal of Photogrammetry Remote Sensing* 66 (3): 247–259. doi:[10.1016/j.isprsjprs.2010.11.001](https://doi.org/10.1016/j.isprsjprs.2010.11.001).
- Periasamy, S. 2018. "Significance of Dual Polarimetric Synthetic Aperture Radar in Biomass Retrieval: An Attempt on Sentinel-1." *Remote Sensing of Environment* 217: 537–549. doi:[10.1016/j.rse.2018.09.003](https://doi.org/10.1016/j.rse.2018.09.003).
- Philipp, M. B., and S. R. Levick. 2020. "Exploring the Potential of C-Band SAR in Contributing to Burn Severity Mapping in Tropical Savanna." *Remote Sensing* 12 (1): 49. doi:[10.3390/rs12010049](https://doi.org/10.3390/rs12010049).
- Quintano, C., A. Fernández-Manso, and O. Fernández-Manso. 2018. "Combination of Landsat and Sentinel-2 MSI Data for Initial Assessing of Burn Severity." *International Journal of Applied Earth Observation and Geoinformation* 64: 221–225. doi:[10.1016/j.jag.2017.09.014](https://doi.org/10.1016/j.jag.2017.09.014).
- Raczko, E., and B. Zagajewski. 2017. "Comparison of Support Vector Machine, Random Forest and Neural Network Classifiers for Tree Species Classification on Airborne Hyperspectral APEX Images." *European Journal of Remote Sensing* 50 (1): 144–154. doi:[10.1080/22797254.2017.1299557](https://doi.org/10.1080/22797254.2017.1299557).
- Schroeder, W., P. Oliva, L. Giglio, and I. A. Csiszar. 2014. "The New VIIRS 375 M Active Fire Detection Data Product: Algorithm Description and Initial Assessment." *Remote Sensing of Environment* 143: 85–96. doi:[10.1016/j.rse.2013.12.008](https://doi.org/10.1016/j.rse.2013.12.008).
- Schroeder, W., E. Prins, L. Giglio, I. Csiszar, C. Schmidt, J. Morissette, and D. Morton. 2008. "Validation of GOES and MODIS Active Fire Detection Products Using ASTER and ETM+ Data." *Remote Sensing of Environment* 112 (5): 2711–2726.
- Sheykhou, M., M. Mahdianpari, H. Ghanbari, F. Mohammadimanesh, P. Ghamisi, and S. Homayouni. 2020. "Support Vector Machine versus Random Forest for Remote Sensing Image Classification: A Meta-Analysis and Systematic Review." *IEEE Journal of Selected Topics in Applied Earth Observations Remote Sensing* 13: 6308–6325. doi:[10.1109/JSTARS.2020.3026724](https://doi.org/10.1109/JSTARS.2020.3026724).
- Tanase, M. A., M. Santoro, P. F. Juan de La Riva, T. Le Toan, and T. Le Toan. 2010. "Sensitivity of X-, C-, and L-Band SAR Backscatter to Burn Severity in Mediterranean Pine Forests." *IEEE Transactions on Geoscience and Remote Sensing* 48 (10): 3663–3675. doi:[10.1109/TGRS.2010.2049653](https://doi.org/10.1109/TGRS.2010.2049653).
- Touzi, R. 2016. "Polarimetric Target Scattering Decomposition: A Review." 2016 IEEE International Geoscience and Remote Sensing Symposium (IGARSS), Beijing, China, 5658–5661. doi:[10.1109/IGARSS.2016.7730478](https://doi.org/10.1109/IGARSS.2016.7730478).
- Vapnik, V. 1999. *The Nature of Statistical Learning theory*: Springer Science & Business Media.
- Verhegghen, A., H. Eva, G. Ceccherini, F. Achard, V. Gond, S. Gourlet-Fleury, and P. Omar Cerutti. 2016. "The Potential of Sentinel Satellites for Burnt Area Mapping and Monitoring in the Congo Basin Forests." *Remote Sensing* 8 (12): 986. doi:[10.3390/rs8120986](https://doi.org/10.3390/rs8120986).
- Washaya, P., T. Balz, and B. Mohamadi. 2018. "Coherence Change-Detection with Sentinel-1 for Natural and Anthropogenic Disaster Monitoring in Urban Areas." *Remote Sensing* 10 (7): 1026. doi:[10.3390/rs10071026](https://doi.org/10.3390/rs10071026).
- Zhang, Y., J. Hui, Q. Qin, Y. Sun, T. Zhang, H. Sun, and L. Minzan. 2021. "Transfer-Learning-Based Approach for Leaf Chlorophyll Content Estimation of Winter Wheat from Hyperspectral Data." *Remote Sensing of Environment* 267: 112724. doi:[10.1016/j.rse.2021.112724](https://doi.org/10.1016/j.rse.2021.112724).
- Zhang, P., A. Nascetti, Y. Ban, and M. Gong. 2019. "An Implicit Radar Convolutional Burn Index for Burnt Area Mapping with Sentinel-1 C-Band SAR Data." *ISPRS Journal of Photogrammetry and Remote Sensing* 158: 50–62. doi:[10.1016/j.isprsjprs.2019.09.013](https://doi.org/10.1016/j.isprsjprs.2019.09.013).